Available online at www.sciencedirect.com
ScienceDirect
International Journal of Thermal Sciences 48 (2009) 85–95
International Journal of Thermal Sciences
www.elsevier.com/locate/ijts

# An empirical validation of window solar gain models and the associated interactions

Peter G. Loutzenhiser [a], Heinrich Manz [a,*], Sven Moosberger [b], Gregory M. Maxwell [c]

[a] *Swiss Federal Laboratories for Materials Testing and Research, Laboratory for Building Technologies, Ueberlandstrasse 129, CH-8600 Duebendorf, Switzerland*
[b] *University of Applied Science of Central Switzerland (HTAL), Department of Architecture and Technology, CH-6048 Horw, Switzerland*
[c] *Iowa State University, Department of Mechanical Engineering, Ames, IA 50011, USA*

Received 16 March 2007; accepted 23 January 2008

Available online 18 April 2008

**Abstract**

An empirical validation of building energy simulation programs was performed in a test cell on the Swiss Federal Laboratories for Materials Testing and Research (EMPA) campus in Duebendorf, Switzerland. The purpose of this exercise was to evaluate the performances of three building energy simulation programs when simulating energy flows through a window (i.e. glazing unit and window frame). The programs used for this study were EnergyPlus, DOE-2.1E, and IDA-ICE. The inputs to the building energy simulation programs were ascertained through precise measurements and simulations, which are explained in detail in this paper. To assess overall performance, the cooling power measured in the experiment was compared with the programs' predictions. Thorough statistical analyses and comparisons were used to determine the impact of experiment output, input uncertainties and evaluate the programs. The absolute average difference between the experiment and predictions for EnergyPlus, DOE-2.1E, and IDA-ICE were 5.8, 9.9, and 6.0%, respectively.


*Keywords:* Empirical validation; Building energy simulation tools; Solar gains

## 1. Introduction

The ability to accurately represent all aspects of a structure is crucial for designing sustainable buildings. Powerful software tools, known as building energy simulation programs, are now being employed by engineers and architects to model heat transfer phenomena (i.e. conduction, convection, and radiation) across the control volumes of modern edifices for optimization of energy consumption and equipment sizing. Given the complexities associated with these phenomena (non-linear, transient, three-dimensional, etc.), assumptions and simplifications must be made in the programs to facilitate computation and allow their application to the design of large buildings. The levels of complexity vary from program to program; the underlying theory and assumptions employed are provided by Clarke [1]. To assess the impact of these assumptions and measure the overall effectiveness of the programs, steps must be taken to evaluate these influences.

The contemporary buildings designed throughout the world often feature highly glazed facades. In terms of thermal transmittance, windows (i.e. glazing unit and window frame) usually represent weak points in the building envelope and the thermal bridges resulting from glazing spacer, window frame, and mounting afford additional modeling challenges to building simulators. Over the past three decades, researchers have struggled to ascertain the sensitivities of models to these assumptions and harnessed increased computing power and advanced experimental apparatus to achieve an accurate quantification of heat transport through windows.

When windows are modeled in building energy simulation programs, the thermal capacitances of the window frames and glazing units are typically neglected, thereby, reducing the complexities of the problem and allowing for steady-state analyses. In most building energy simulation programs, conduction through the window is modeled in one-dimension and corrections are then used to factor in thermal bridging.

* Corresponding author. Tel.: +41 44 823 4790; fax: +41 44 823 4009.
*E-mail address:* heinrich.manz@empa.ch (H. Manz).

1290-0729/$ – see front matter 
doi:10.1016/j.ijthermalsci.2008.01.011

**Nomenclature**

| | |
|---|---|
| $A$ | area |
| $c$ | specific heat |
| $D$ | measured and predicted difference vectors |
| $d$ | distance or width |
| $k$ | thermal conductivity |
| $L$ | height of given element |
| $OU$ | overall uncertainty |
| $P$ | total length of perimeter |
| $R$ | combined radiative and convective surface resistance |
| $s$ | sample standard deviation |
| $t$ | time |
| $Q$ | total heat transfer |
| $Q'$ | heat flow per unit length |
| $\dot{q}$ | heat generation |
| $U$ | thermal transmittance of element |
| $(UA)$ | overall thermal transmittance of element |
| $UR$ | uncertainty ratio |
| $x$ | vector of containing measured or predicted cooling power or coordinate direction |
| $y$ | coordinate direction |

*Subscripts*

| | |
|---|---|
| $c$ | cold side of hotbox |
| $e$ | eps foam |
| edge | edge effects |
| exp | experiment |
| $g$ | exposed glazing unit |
| $h$ | hot side of hotbox |
| hb | hotbox |
| $i$ | inner zone for two-dimensional simulation |
| ins | insulation panel simulation |
| $j$ | given hour of experiment |
| $m$ | window mounting |
| max | maximum value of vector |
| min | minimum value of vector |
| $o$ | outer zone for two-dimensional simulation |
| $p$ | plywood |
| rms | root mean squared |
| sp | window spacer |
| wall | entire wall composite excluding window |
| wf | window frame |
| mca | Monte Carlo Analysis |
| 1D | one-dimensional |
| 95% | 95$^{th}$ percentile |

*Greek symbols*

| | |
|---|---|
| $\theta$ | temperature |
| $\varphi$ | linear thermal transmittance |
| $\Lambda$ | conductance |
| $\rho$ | density |

When analyzing the glazing unit, the outer and inner surfaces are usually represented as isothermal surfaces. For modeling convection, average convective heat transfer coefficients are used in conjunction with details of the orientation of the construction elements, in this case windows. More recent programs make use of advanced flat plate correlations that assume a boundary layer regime (laminar or turbulent) and empirically, numerically, or analytically derived, time-varying correlations that are functions of air temperatures, boundary layer length and surface orientation [2,3]. For outside convective heat transfer, wind velocity and direction offer additional levels of accuracy. When accounting for longwave radiation, the associated heat transfer is modeled in varying levels of detail. For more advanced programs, analytical, numerical, and/or approximate diffuse viewfactors are computed and used in conjunction with energy balances and surface emittance. However, many of the simpler programs combine internal longwave radiation and convection heat flux calculations into heat transfer coefficients that are design standards or functions of surface orientations. These heat transfer coefficients remain constant during the entire simulation.

Shortwave radiation through windows is modeled using advanced measurements [4], glazing databases [5–7], and algorithms [8–11] that allow quantification of the optical properties of glazing, including angular-dependent solar and visible transmittances and reflectances. These measurements coupled with computations and measurements of center-of-glazing thermal transmittances (also known as $U$-values or $U$-factors) can be used to accurately describe a glazing unit.

Assessing the overall impact of the window requires advanced consideration of edge-effects and window frames, which add further levels of complexity. A variety of calculation procedures are used in different parts of the world to quantify these effects. Overviews and comparisons of these calculation procedures are given by [12,13]. In determining the window spacer and frame effects, two-dimensional heat transfer simulation and/or experimental analyses substantially increase the accuracies. Previous studies in these areas were performed by [13–22].

Transient one-dimensional heat transfer conduction plus appropriate thermophysical properties are usually assumed for representation of the remaining heat transfer elements—walls, ceilings and floors—in more advanced programs. Most building energy simulations use either response functions or numerical modeling to represent transient conduction [1]; allowance is made for longwave radiation and convective heat flux using the same methodology described for the glazing unit boundary layers and/or surfaces.

Validation exercises are essential in assessing the performance of the building energy simulation programs. Three types of validation procedures are identified along with a full description of the advantages and disadvantages by [23,24]. The identified procedures are: (1) analytical, i.e. comparing the results of the programs to known analytical solutions, (2) program-to-

program comparisons, i.e. specifying exact inputs and comparing program outputs, and (3) empirical, i.e. modeling a well-instrumented facility and comparing experimental and program outputs. Methodologies and empirical validations performed in International Energy Agency (IEA) Tasks and Annexes [25–29] and in the PASSYS project [30,31] provided a crucial foundation for this research.

The test cell used in this study is located on the Swiss Federal Laboratories Materials Testing and Research (EMPA) campus in Duebendorf, Switzerland. Previous research focused on evaluating the transient characteristics and thermal bridges of the test cell [32], assessing tilted facade radiation models [33] and evaluating solar gain models and interactions in a glazing unit [34] with internal and external shading screens [35] and internal and external blinds [36]. The exercise described in this paper is the last in a series of experiments and validation exercises performed within the scope of IEA Task 34/Annex 43 Project C. The empirical validation exercise was carried out to evaluate solar gains through a window and the associated interactions. The test cell is well-instrumented, with over 200 sensors, and was designed with guard zones for careful control of the boundary conditions. The use of test cells allows the precise control and monitoring of boundary conditions while creating an environment similar to an office space (i.e. thermophysical properties, dimensions, and airflow patterns). This makes them ideal for empirical validations of building energy simulation programs. The data acquired from this facility meet all nine criteria specified by [26] for high quality data sets.

For this validation exercise, a window was installed in the exterior construction element of the test cell and models were constructed in EnergyPlus [37], DOE-2.1E [38], and IDA-ICE [39]. The cooling power required to maintain a near-constant temperature in the test cell was measured during the experiment and compared with results from the building energy simulation programs. The optical properties of the glazing unit in the window were quantified and detailed analyses were performed of the window spacer and frame coupling calorimetric measurements from a calorimetric hotbox with results from two-dimensional heat transfer simulations. The results are accompanied by robust statistical and sensitivity analyses to gauge the accuracies of the programs and assess the impact of experimental uncertainties.

## 2. Experiment

The experiment was run in the EMPA test cell with a window installed for a 20-day period from June 30 to July 19, 2006. During this time, the facade was exposed to diverse atmospheric conditions. The purpose of the validation exercise was to evaluate the impact of solar gains through a window and associated interactions by examining the cooling power required to maintain a fixed air temperature, measured by 18 double-shielded thermocouples. Conditioned air was supplied to the test cell via two textile ducts at very low velocities near the floor and extracted through the ceiling to reduce temperature stratification.

Fig. 1. Photograph of the test cell taken during the experiment.

Information on the facility and inputs required for the building energy simulation program are provided in this section. A photograph of the facility taken during the test is shown Fig. 1.

### 2.1. Facility

The EMPA test cell is located just outside of Zurich in Duebendorf, Switzerland (8.6 °E, 47.4 °N; 430 m ASL, GMT + 1 h). The exterior vertical construction element faces 29° west of south. Detailed information on the thermophysical and surface optical properties of the construction elements and test cell geometry are given by [32]. The facility also contains an advanced weather monitoring station. To ensure uniform ground reflectance, green artificial turf was installed in front of the test cell and the solar reflectance quantified by [33].

### 2.2. Window

The window chosen for this experiment was composed of a wood frame and a solar selective, insulating glazing unit with a stainless steel spacer and an argon-filled cavity. A thorough appraisal of the window was performed and is described in subsequent sections.

#### 2.2.1. Optical properties

The transmittances and inner and outer reflectances of the glazing unit and the individual glass panes were measured using a spectrometer from 250 to 2500 nm. The outer pane in the glazing unit was of clear float glass and the inner pane of glass with a low-emittance coating on one side. Fig. 2 shows a plot of the transmittances and inner and outer reflectance as a function of wavelength. The transmittances and reflectances for the glazing unit and glass panes were integrated over the solar spectrum in accordance with EN 410 [40] using Glad software [6], and the outer and inner hemispherical emittances of the glass panes were measured using an emissometer based on a calorimetric method; these values are presented in Table 1.

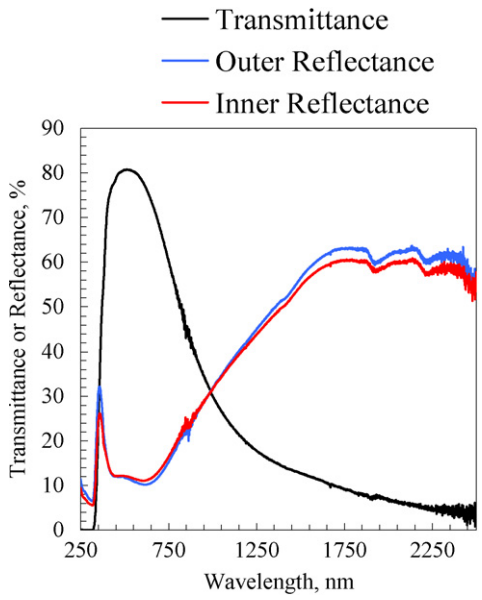


Fig. 2. Measured transmittances and reflectances of the window.

### 2.2.2. Thermal transmittances and bridges

A BISCO [41] simulation and calorimetric hotbox measurements were used in combination to divide the heat transfer between the window components. The governing relationship for heat transfer through a solid element, Fourier's law, is given in its full form in Eq. (1). The BISCO software uses a triangular grid structure to solve the energy equation in combination with Fourier's law assuming steady-state conditions. The two-dimensional analysis further assumes no heat sources and sinks and constant thermal conductivity, which reduces to Laplace's equation, given in Eq. (2) in Cartesian coordinates. For the simulation, a control volume was defined around each node and the system of equations was solved iteratively. The grid was refined until it was certain that independence was achieved.

$$\rho c \frac{\partial \theta}{\partial t} = \mathrm{div}(k \nabla \theta) + \dot{q} \tag{1}$$

$$\frac{\partial^2 \theta}{\partial x^2} + \frac{\partial^2 \theta}{\partial y^2} = 0 \tag{2}$$

The results from the thermal bridge calculations with the center-pane thermal transmittance and conductance of the window described in this section are summarized in Table 2. The theory behind the calculation of these quantities is developed in subsequent sections. By way of comparison, Table 2 also contains generic thermal transmittances taken from the standard values in Glad Software [6] that are used by simulators without access to powerful heat transfer simulation tools and hotboxes. This highlights the importance in an empirical validation of accurately specifying as many quantities as possible. The percent errors, also given in Table 2, were computed to show the importance of thorough quantification.

A cross-section of the glazing unit, window frame, and mounting is shown in Fig. 3. The thermal conductivities were taken from literature and in-house measurements; the temperature-dependent thermophysical properties were fixed as the average between the outer and inner air temperatures for the southwest wall.

### 2.2.3. Linear thermal transmittance of the spacer

The impact of the spacer was calculated using a two-dimensional drawing of the spacer/frame assembly. The linear thermal transmittance of the spacer was evaluated based on prEN ISO 10077-2 [42]. However, some modifications were made in the calculation procedure to compute more precise quantities. During the hotbox measurements, the heat flux through the center of the window pane was measured and a center-pane thermal transmittance was then computed. Using this measurement, an equivalent conductivity was computed for the argon-filled glazing cavity that factored in the impact of conduction, convection, and radiation. The thermal transmittance was also used to compute an equivalent thermal conductivity of the insulation panel [42] for replacing the glazing unit in the frame as (deviating slightly from [42], which specifies a fixed equivalent thermal conductivity). Equivalent thermal conductivities were calculated for the air cavities and the conditions of the inside

Table 1
Optical properties of window

| Parameter | Glazing unit | Outer glass pane | Inner glass pane |
|---|---|---|---|
| Normal solar transmittance, % | 53.7 ± 1 | 83.6 ± 1 | 62.5 ± 1 |
| Normal solar exterior reflectance, % | 23.3 ± 1 | 7.8 ± 1 | 24.9 ± 1 |
| Normal solar interior reflectance, % | 22.4 ± 1 | 7.7 ± 1 | 20.0 ± 1 |
| Outer emittance, % | – | 85.3 ± 5 | 8.5 ± 5 |
| Inner emittance, % | – | 87.3 ± 5 | 87.3 ± 5 |

Table 2
Computed and measured thermal bridge and center-pane glazing properties compared with standard values taken from [6]

| Description | Quantity | Standard values | Percent error |
|---|---|---|---|
| Center-pane thermal transmittance of glazing unit | 1.163 W/m$^2$ K ± 5% | 1.3 W/m$^2$ K | 11.8% |
| Center-pane thermal conductance of glazing unit | 1.449 W/m$^2$ K ± 5% | | |
| Linear thermal transmittance for spacer | 0.073 W/m K ± 5% | 0.05 W/m K | 31.5% |
| Thermal transmittance of window frame | 1.285 W/m$^2$ K ± 5% | 1.45 W/m$^2$ K | 12.8% |
| Thermal conductance of window frame | 1.643 W/m$^2$ K ± 5% | | |
| Linear thermal transmittance for mounting | −0.028 W/m K ± 5% | | |

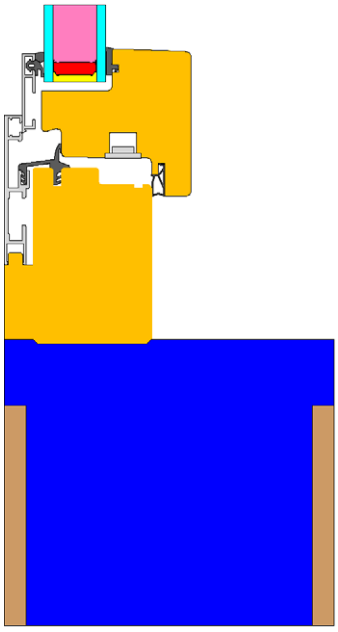

Fig. 3. Drawing of the spacer and window frame.

and outside boundaries according to [42]. The linear thermal transmittance due to the spacer was computed using Eq. (3) with results from the BISCO simulations. During the simulation, the exposed area of the glazing unit that extended out from the window frame was 0.550 m to ensure that all edge effects of the thermal bridges were captured.

$$\psi_{\mathrm{sp}} = \frac{Q'_{\mathrm{sp}} - Q'_{\mathrm{ins}}}{\theta_i - \theta_o} \tag{3}$$

*2.2.4. Thermal conductance of the window frame*

The thermal transmittance of the window frame was computed using the BISCO simulation, the spacer linear thermal transmittance of the spacer, one-dimensional steady heat transfer, and the principle of superposition. For this calculation, the window frame height was fixed, and linear temperature profiles were assumed across the window frame for the steady one-dimensional heat transfer. The thermal transmittance and conductance of the window frame were calculated using Eqs. (4) and (5), respectively. The thermal conductance was a necessary calculation due to the different heat transfer coefficients in simulation and hotbox measurement. The frame conductance was also an important input into the building energy simulation programs, which all had at least one dynamic convective surface heat transfer correlation.

$$U_{\mathrm{wf}} = \frac{\frac{Q'_{\mathrm{sp}}}{\theta_i - \theta_o} - \psi_{\mathrm{sp}} - L_g U_g}{L_{\mathrm{wf}}} \tag{4}$$

$$\Lambda_{\mathrm{wf}} = \left[U_{\mathrm{wf}}^{-1} - R_i - R_o\right]^{-1} \tag{5}$$

*2.2.5. Linear thermal transmittance due to mounting*

The linear thermal transmittance due to the mounting of the window in the frame was computed by coupling BISCO simulation results with hotbox measurements. The results used for the calculation also included thermal bridges from the spacer and window frame; non-homogeneities (i.e. screws and frames) and corner effects from the window frame and spacer were neglected. For this calculation, the outer wall was assumed to be composed entirely of homogeneous layered material specified for the building energy simulation programs; the actual window mounting construction (Fig. 3), however, exhibited greater thermal resistance. The hotbox measurements were also considered quasi-steady state while the one-dimensional calculations assumed linear temperature profiles across each material. Measured film coefficients measured in the experiment were applied in these computations instead of the combined heat transfer coefficients used in the simulations. Eq. (6) was used to calculate the one-dimensional overall thermal transmittance through the window frame, outside wall, and glazing unit. Temperature-dependent thermophysical properties were fixed at the mean temperature of the hot and cold chambers.

$$\begin{aligned}(UA)_{\mathrm{1D}} = {} & A_{\mathrm{wall}}\left(R_c + \frac{2d_p}{k_p} + \frac{d_e}{k_e} + R_h\right)^{-1} \\ & + A_{\mathrm{wf}}\left(R_c + \frac{1}{\Lambda_{\mathrm{wf}}} + R_h\right)^{-1} \\ & + A_g\left(R_c + \frac{1}{\Lambda_g} + R_h\right)^{-1}\end{aligned} \tag{6}$$

The linear thermal transmittance of the mounting was calculated using Eq. (7). The negative value (Table 2) indicated that the thermal resistance in one-dimension plus the additional thermal bridging from the spacer and frame was less than the measurements.

$$\psi_m = \frac{\frac{Q_{\mathrm{hb}}}{\theta_h - \theta_c} - (UA)_{\mathrm{1D}} - \psi_{\mathrm{sp}} P_{\mathrm{sp}}}{P_m} \tag{7}$$

An additional simulation run was carried out to examine the heat flow through the element with the window frame mounting. A drawing with heat flow lines is shown in Fig. 4.

## 3. Simulations

This experiment was modeled using three simulation programs: EnergyPlus, DOE-2.1E, and IDA-ICE. The temperature-dependent thermophysical properties described by [32] were fixed at the mean construction element temperature for the experiment. The measured outer surface temperatures for the elements adjacent to the guarded zones, air temperatures, and internal loads, which included the fans and miscellaneous electrical equipment in the test cell, were used as inputs in hourly increments to the programs. The average and standard deviation computed over the experiment of the space-averaged air temperature and internal loads were $22.57 \pm 0.10\,^{\circ}\mathrm{C}$ and $180.09 \pm 0.89$ W, respectively.

Previous work by [33] revealed the Perez 1990 model [43] for predicted solar irradiance on tilted facades to be the best model for the region; all three building energy simulation programs consequently used this model along with two of the three solar irradiance components measured at the facility (direct-normal and global horizontal and diffuse). The programs also all contained optical models that used normal transmittances

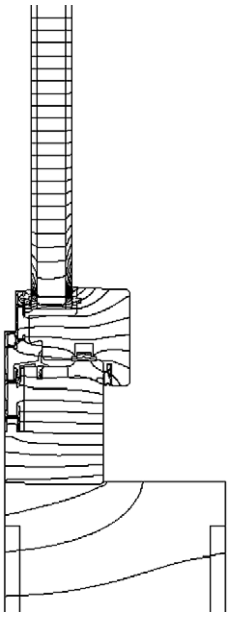

Fig. 4. Heat flow lines from the BISCO simulation.

and reflectances to compute angular-dependent values. Narratives of the specific modeling procedures employed for each program are presented in the following sections.

### 3.1. EnergyPlus

The window was modeled in EnergyPlus by defining two panes of glass. Measured reflectances and transmittances for each pane of glass from 250 or 2500 nm were input together with hemispherical emittances. Because the algorithm used to compute the center-pane thermal conductance over-predicted the measured/simulation results, the thermal conductivities of the glass panes were reduced to match the quantities in Table 2. Both the linear thermal transmittance due to the mounting and the external wall thermal bridge were included in the overall window frame conductance. A different standard was used in EnergyPlus to account for the edge effects. This defined an edge area up to 0.0635 m from the frame and specified the program input as the ratio of the edge conductance to the center-pane conductance. The edge conductance was calculated using Eq. (7), which factored in the linear transmittance of the spacer and the thermal conductance through the edge area. The same procedure was used to allow for the linear thermal transmittance due to mounting and the external thermal bridge described by [32] in the window frame computations.

$$\Lambda_{\text{edge}} = \left\{ \left( \frac{P_{\text{sp}}\psi_{\text{sp}}}{A_{\text{edge}}} + U_g \right)^{-1} - R_i - R_o \right\}^{-1} \tag{8}$$

Measured direct-normal and diffuse horizontal solar irradiances were used to compute global vertical solar irradiance on the outer surface of the facade and window. Six hourly timesteps were set and the hourly averaged results compared. A dynamic convective heat transfer correlation was used to factor in boundary layer length, orientation, and air and surface temperature differences. Approximate diffuse view factors were computed and used in conjunction with an energy balance to account for internal longwave radiation exchange. The procedures and algorithms are given by [44].

### 3.2. DOE-2.1E

The window was defined in DOE-2.1E using a Window 5.2 [45] output file with a modified center-pane thermal transmittance. Wavelength-dependent measurements for the front and back reflectances and transmittances, and hemispherical emittances for each glass pane were imported into a user's database of Optics 5 [46]. From Optics, the information was accessed by Window 5.2, and the window was then modeled. The center-pane thermal transmittance was used for the entire glazing unit and all thermal bridges, including those associated with spacer, mounting and external thermal bridge [32], were included in the window frame conductance as shown in Eq. (8).

$$\Lambda_{\text{wf,DOE-2}} = \left\{ \left( \frac{P_{\text{sp}}\psi_{\text{sp}} + P_m\psi_m + (UA)_{eb}}{A_{\text{wf}}} + U_{\text{wf}} \right)^{-1} - R_i - R_o \right\}^{-1} \tag{9}$$

Measured direct-normal and global horizontal solar irradiances were used to calculate global vertical solar irradiances. The weather data were accessed by the program in hourly TMY2 format. Because infrared global irradiance is not explicitly described in TMY2 weather format, an opaque cloud cover modifier was computed by reversing the algorithm used in DOE-2.1E. Fixed combined heat transfer coefficients for interior surfaces were used based on design recommendations given by [47].

### 3.3. IDA-ICE

The window was simulated using the new Detwind model based on ISO-15099 [48]. This model was employed to compute overall heat transfer through the glazing and all window parameters. The parameters for the window panes and gas filling were determined by the model using the provided window properties data. The thermal transmittance of the window frame was directly input together with the thermal bridges due to frame mounting and linear thermal transmittance of the spacer. Allowance was made for the shading effect of the window frame itself by shifting the center glazing pane 0.04 m inside the external facade surface.

Measured hourly direct-normal and diffuse horizontal solar irradiances were used to compute the tilted facade solar irradiance. The longwave radiative heat transfer was simulated using view factors. A dynamic convective heat transfer coefficient algorithm was used to factor in the construction element orientation and air and surface temperature differences.

## 4. Sensitivity study

A prerequisite for any empirical validation is careful consideration of all elements of experimental uncertainty. For this

Table 3
Average overall uncertainty and 10 most influential input parameters from factorial analyses impacting cooling power, in W

| Parameter | Forward | Backward |
|---|---|---|
| Overall uncertainty | 3.39 | 3.40 |
| Average air temperature | −1.88 | 1.88 |
| Fan power | 1.04 | −1.04 |
| West wall outer surface temperature | 0.79 | −0.79 |
| Ceiling outer surface temperature | 0.73 | −0.73 |
| North wall outer surface temperature | 0.69 | −0.69 |
| East wall outer surface temperature | 0.56 | −0.56 |
| Outside air temperature | 0.56 | −0.56 |
| Direct-normal solar irradiance | 0.55 | −0.56 |
| Diffuse horizontal solar irradiance | 0.47 | −0.50 |
| Front reflectance inner glass Pane | −0.43 | 0.42 |

Table 4
Average overall uncertainty and 10 most influential input parameters from factorial analyses, computed only when sun was up, that impacted cooling power, in W

| Parameter | Forward | Backward |
|---|---|---|
| Overall uncertainty | 3.73 | 3.74 |
| Average air temperature | −1.94 | 1.94 |
| Fan power | 1.04 | −1.04 |
| West wall outer surface temperature | 0.82 | −0.82 |
| Direct-normal solar irradiance | 0.76 | −0.78 |
| Ceiling outer surface temperature | 0.75 | −0.75 |
| North wall outer surface temperature | 0.70 | −0.71 |
| Diffuse horizontal solar irradiance | 0.66 | −0.69 |
| Front reflectance inner glass pane | −0.60 | 0.60 |
| Outside air temperature | 0.58 | −0.58 |
| East wall outer surface temperature | 0.58 | −0.59 |

study, measured and predicted cooling powers were used to assess program performance. The uncertainty of the measuring was estimated as ±2% using manufacturers' specifications. $N$-way factorial analysis for fitted effects and Monte Carlo Analysis (MCA) were used to quantify the impact on predicted cooling power of the input uncertainties propagated through the building energy simulation programs. For this study, the analyses were performed only in EnergyPlus; a description of its implementation is given by [33]. A quantification and methodology for the computation of uncertainties due to weather data, optical properties, thermophysical properties, thermal bridges, air and outer surface temperatures, and ground reflectance are given in Tables 1 and 2 and by [32–34]. Results from both analyses are presented in this section.

### 4.1. $N$-way factorial analysis

An $N$-way Factorial Analysis was performed for all hours of the experiment to evaluate the sensitivity of the cooling power to individual inputs and confirm linear responses over the uncertainty range. This was required for application of the Central Limit Theorem to the MCA; therefore, both forward and backward differencing was performed. The average uncertainty over the entire test period was computed and is displayed in Table 3 along with the 10 most influential factorials. However, the impact of solar irradiance inputs was somewhat mitigated in these analyses due to the absence of effects after the sun has set. Hence, the average overall uncertainty and the 10 most sensitive parameters were recomputed omitting the results obtained when the solar altitude was less than zero (when the sun was down). As expected, the uncertainties in the solar irradiance measurements become much more significant. Yet, the cooling power predictions remained very sensitive to surface temperature and air temperature uncertainties.

### 4.2. Monte Carlo analysis

The MCA was run every hour to ascertain the propagation of error through the building energy simulation program. One-hundred twenty runs were used for the MCA in this study. The average overall uncertainty and the average uncertainty omitting predictions when the solar altitude was less than zero for the cooling power were 3.22 and 3.57 W, respectively. These figures are largely consistent with the results from the $N$-way factorial analyses (forward and backward differencing). To verify Gaussian distributions, it was demonstrated by means of Lillefors Tests that there was no evidence at a 1% significance level that the outputs were not normally distributed for all hours of the experiment except one. The hourly results from the MCA were used in conjunction with the experimental uncertainty to compute 95% credible limits to assess the building energy simulation programs' performances.

## 5. Results

The comparisons made for this empirical validation exercise focused on the cooling power within the test cell. Cooling power was required at all times due to the high internal loads from the fans. This parameter supplies all the information needed to estimate the performance of the heat transport algorithms and their interaction within the respective programs. Plots were generated to compare the results from the experiments.

Cooling power plots were constructed for each building energy simulation program to compare the predicted results with measurings taken from the test cell. Two plots were constructed for each program to show the results. For presentation purposes, the plot on the left contains cooling power averaged over every hour of day for each day of the experiment. Ninety-five percent credible limits from the experimental error analysis and MCA were also averaged over every hour of the day and are applied to the experimental results and program predictions respectively. The plot on the right contains maximum, mean, and minimum absolute differences for each hour of the day during the experiment. The results for EnergyPlus, DOE-2.1E, and IDA-ICE are shown in Figs. 5, 6, and 7, respectively.

The cooling powers were compared using the statistical analysis procedure proposed by [32]. An important quantity that factors in uncertainty with the difference between the measured and predicted comparisons is the uncertainty ratio given in Eq. (9). When the uncertainty ratio is less than unity, the

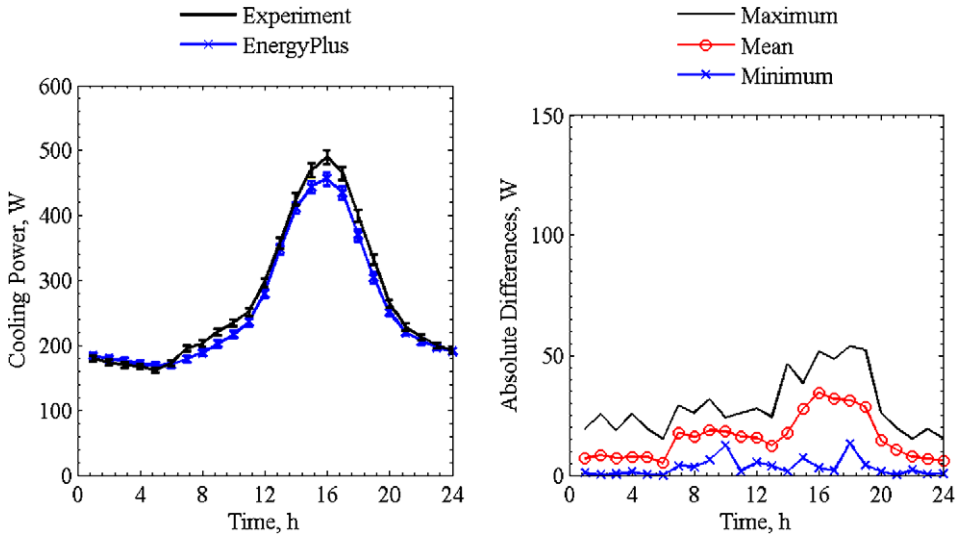


Fig. 5. Cooling power comparisons for EnergyPlus averaged over each given hour of the day (left) and absolute maximum, mean and minimum differences for a given hour of the day (right).

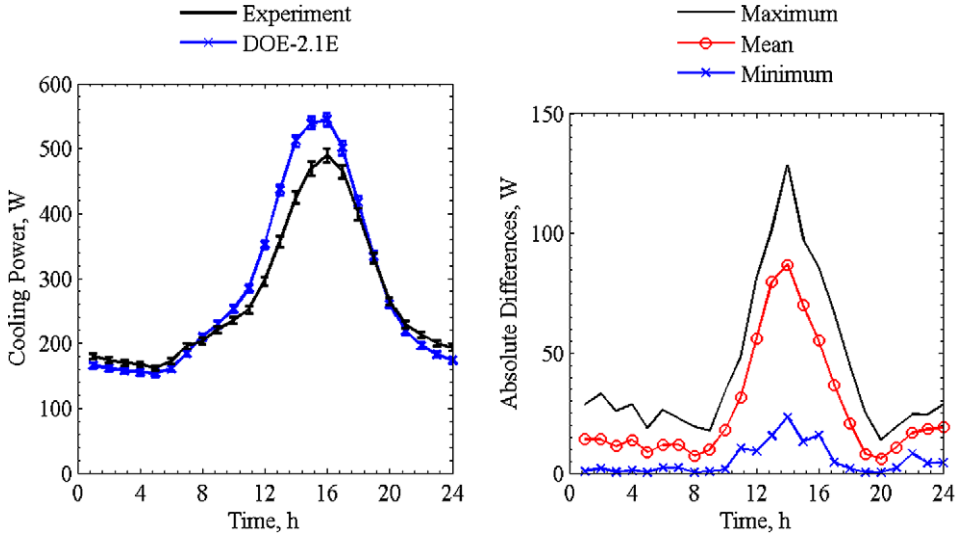


Fig. 6. Cooling power comparisons for DOE-2.1E averaged over each given hour of the day (left) and absolute maximum, mean and minimum differences for a given hour of the day (right).

predictions are within overlapping 95% credible limits. Table 5 contains the results from the statistical analyses performed for the entire experiment and when the solar altitude was greater than zero.

$$UR_j = \frac{|D|_j}{OU_{\mathrm{exp},j} + OU_{\mathrm{mca},j}} \tag{10}$$

A comparison of the transmitted solar power through the glazing unit of the window was also performed and the results, averaged over each given hour of the day for the entire experiment, are shown in Fig. 8. No empirical data were available for comparisons to this parameter because it was not measured in the experimental setup. However, this comparison provides constructive insight for identifying differences in the optical models used by the building energy simulation programs accounting for differences in the predictions.

## 6. Discussion

Strictly speaking, none of the building energy simulation programs were validated within overlapping 95% credible limits over the entire simulation as prescribed by the uncertainty ratio. However, the average difference computed over the entire test for EnergyPlus (−11.7 W) was within the sum of average overall 95% credible limits (6.1 W + 6.3 W = 12.4 W). For all programs, the results over the entire experiment were slightly better than the truncated analyses that omitted comparisons when the sun was down, indicating the programs had greater difficulty representing shortwave radiation. However, the cell time constant was 17 hours [32]; therefore, solar gains also impacted night-time cooling powers.

The average overall prediction differences ($\bar{D}$ in Table 5) over the entire experiment for EnergyPlus, DOE-2.1E, and IDA-ICE were −4.3, 4.9, and 5.4%, respectively. This is use-

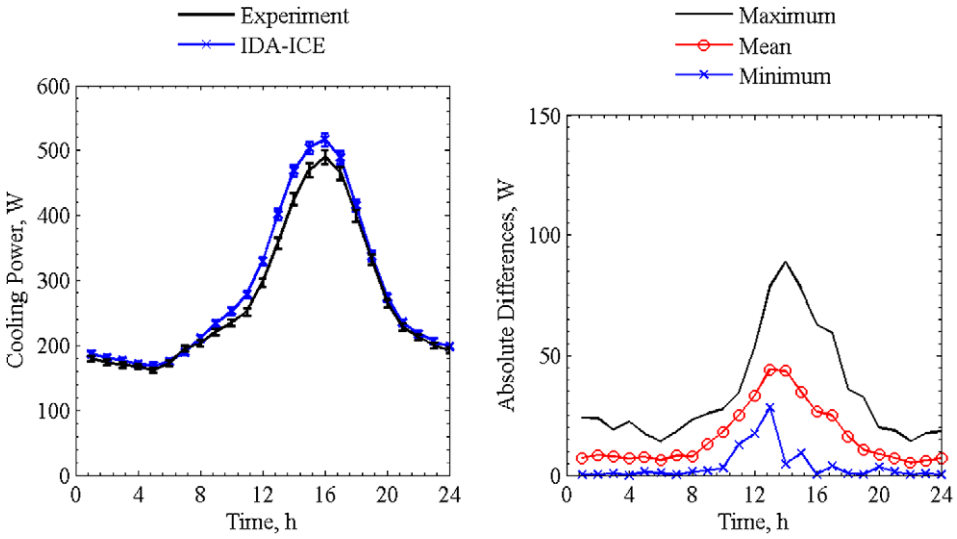


Fig. 7. Cooling power comparisons for IDA-ICE averaged over each given hour of the day (left) and absolute maximum, mean and minimum differences for a given hour of the day (right).

Table 5
Summary of cooling power statistics and comparisons evaluated over entire experiment and when solar altitude was greater than zero

| | Evaluated over entire experiment | | | | Evaluated when sun was up | | | |
|---|---|---|---|---|---|---|---|---|
| | Experiment | EnergyPlus | DOE-2.1E | IDA-ICE | Experiment | EnergyPlus | DOE-2.1E | IDA-ICE |
| $\bar{x}$ | 269.5 W | 257.8 W | 282.8 W | 284.1 W | 304.1 W | 287.1 W | 329.0 W | 322.2 W |
| $s$ | 112.8 W | 101.4 W | 141.5 W | 121.0 W | 117.1 W | 107.3 W | 144.4 W | 124.6 W |
| $x_{max}$ | 576.2 W | 524.5 W | 637.0 W | 585.0 W | 576.2 W | 524.5 W | 637.0 W | 585.0 W |
| $x_{min}$ | 133.1 W | 158.0 W | 143.0 W | 155.5 W | 140.5 W | 158.0 W | 143.0 W | 155.5 W |
| $\bar{D}$ | – | −11.7 W | 13.3 W | 14.5 W | – | −17.0 W | 24.8 W | 18.1W |
| $\overline{\lvert D \rvert}$ | – | 15.7 W | 26.6 W | 16.0 W | – | 19.1 W | 31.2 W | 19.8 W |
| $D_{max}$ | – | 54.0 W | 128.4 W | 88.5 W | – | 54.0 W | 128.4 W | 88.5 W |
| $D_{min}$ | – | 0.0 W | 0.2 W | 0.0 W | – | 0.0 W | 0.2 W | 0.2 W |
| $D_{rms}$ | – | 19.7 W | 37.7 W | 22.5 W | – | 22.7 W | 43.4 W | 26.2 W |
| $\lvert D \rvert_{95\%}$ | – | 40.8 W | 88.0 W | 52.1 W | – | 43.2 W | 93.0 W | 54.6 W |
| $\overline{OU}$ | 6.1 W | 6.3 W | – | – | 6.9 W | 7.0 W | – | – |
| $\overline{UR}$ | – | 1.2 | 1.9 | 1.2 | – | 1.3 | 2.0 | 1.4 |
| $UR_{max}$ | – | 3.4 | 6.6 | 6.1 | – | 3.2 | 6.6 | 6.1 |
| $UR_{min}$ | – | 0.0 | 0.0 | 0.0 | – | 0.0 | 0.0 | 0.0 |
| $\overline{\lvert D \rvert}/\bar{x} \times 100\%$ | – | 5.8% | 9.9% | 6.0% | – | 6.3% | 10.3% | 6.5% |
| $\bar{D}/\bar{x} \times 100\%$ | – | −4.3% | 4.9% | 5.4% | – | −5.6% | 8.2% | 6.0% |

ful for assessing long-term energy consumption predictions. The absolute average overall prediction differences ($\overline{|D|}$ in Table 5) for the entire experiment can be used to evaluate power predictions and for equipment sizing. The absolute average differences for this test were 5.8% for EnergyPlus, 9.9% for DOE-2.1E, and 6.0% for IDA-ICE.

Given the nature of the study and data volume, hourly cooling power measurements and predictions were not plotted in this paper. However, careful inspection of the plotted hourly results showed EnergyPlus to under-predict the cooling power during sunny periods while delivering more accurate predictions for cloudy periods. DOE-2.1E over-predicted the results during the day (sunny or cloudy periods) and slightly under-predicted the results at night. IDA-ICE accurately predicted the results during sunny periods and over-predicted the results at times when only diffuse solar irradiance was present. Both EnergyPlus and IDA-ICE accurately predicted cooling powers during the night. Despite the complexities associated with the window, the accuracy of the night-time predictions shows the methodology involving steady-state coupling of simulation and hotbox measurements to have been appropriate.

As can be seen in Fig. 8, the predictions of solar power transmitted through the glazing unit were quite similar for all three programs. The differences between the optical models were minor and the selection of different solar irradiance components seemed inconsequential. Hence, differences in the cooling power predictions were primarily due to differences in the modeling of longwave and convective heat transport inside the test cell and at the exterior surfaces as well the absorptions and reflections of the shortwave radiation penetrating the test cell through the glazing unit onto the internal surfaces. The programs that performed best for this study (EnergyPlus and IDA-ICE) both featured dynamic convective heat transfer coefficient algorithms and more accurate longwave radiation

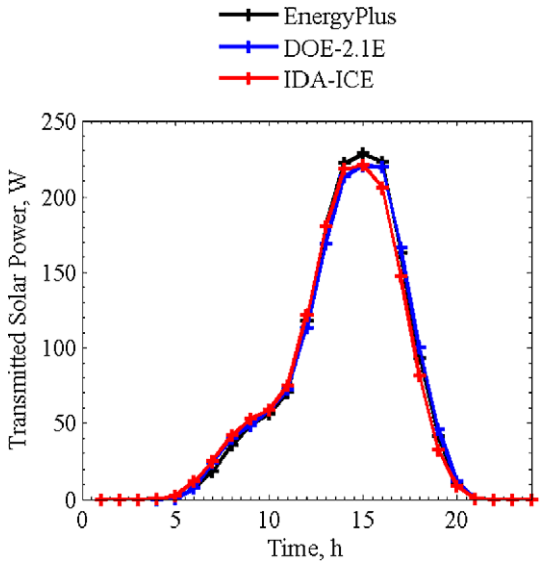


Fig. 8. Transmitted solar power averaged over each hour of the day.

models. Concerns first posed by [49] and reiterated by [34] concerning the simulation of internal convective heat transfer still seem to present significant challenges. More robust modeling of convection and radiation seem to better represent the actual phenomena, which was very apparent during the night in the absence of sunlight the space.

## 7. Conclusions

Despite the simplifications made in the building energy simulation programs, the predictions still accurately represent reality. This validation exercise also provided valuable insights into the impact of various assumptions, particularly concerning the modeling of internal convection and radiation exchange. The primary advantage of this type of validation effort is that all aspects of the experiment, including program inputs and boundary conditions, were carefully controlled. This provided a unique opportunity to assess actual performance of the building energy simulation programs while minimizing experimental uncertainties. Table 2 provides a glimpse of shortcomings introduced into the building energy simulation programs when relying on standard computing methods proposed in codes and standards for quantification of the various window components. This makes datasets such as these all the more important for those researchers and engineers meticulously seeking to improve the capacities of building energy simulation programs. The results from this exercise pinpoint inadequacies in building energy simulation programs and provide guidance for future research directed at improving the overall program performance. The experimental inputs and results from this exercise are now available for download at www.empa.ch/ieatask34.

## Acknowledgements

We acknowledge with thanks the financial support of the Swiss Federal Office of Energy (BFE) for building and testing the experimental facility (Project 17'166) and in funding EMPA's participation in IEA Task 34/43 (Project 100'765). We should like to thank 4B Bachmann for providing the window free of charge. Numerous IEA Task 34/Annex 43 participants provided valuable input for this project. We also wish to thank our colleagues at EMPA—M. Amberg, B. Binder, R. Blessing, S. Carl, T. Frank, and R. Vonbank—for their valuable contributions. We would also like to acknowledge the contributions made by G. Zweifel from HTAL.

## References

[1] J.A. Clarke, Energy Simulation in Building Design, second ed., Butterworth Heinemann, 2001.
[2] C. Cuevas, A. Fissore, Natural convection at an indoor glazing surface, Building and Environment 39 (2004) 1049–1053.
[3] S. Fohanno, G. Polidori, Modelling of natural convective heat transfer at an internal surface, Energy and Buildings 38 (2006) 548–553.
[4] R. Steiner, P. Oelhafen, G. Reber, A. Romanyuk, Experimental determination of spectral and angular dependent optical properties of insulating glasses, in: Proceedings of CISBAT 2005 EPFL, 2005, pp. 441–446.
[5] International Glazing Database Version 15.1, http://windows.lbl.gov/materials/IGDB (retrieved February 8, 2007).
[6] GLAD Software, Swiss Federal Laboratories for Materials Testing and Research (EMPA), Duebendorf, Switzerland, 2002.
[7] WIS, Window Information System, http://windat.ucd.ie/wis/html/index.html, 2002.
[8] R.A. Furler, Angular dependence of optical properties of homogenous glasses, ASHRAE Transactions 97 (2) (1991) 1129–1137.
[9] M. Rubin, R. Powles, K. Von Rottkay, Models for the angle-dependent optical properties of coated glazing materials, Solar Energy 66 (1999) 267–276.
[10] J. Karlsson, M. Rubin, A. Roos, Evaluation of predictive models for the angle-dependent total solar energy transmittance of glazing materials, Solar Energy 71 (2001) 22–31.
[11] A. Roos, P. Polato, P.A. Van Nijnatten, M.G. Hutchins, F. Olive, C. Anderson, Angular-dependent optical properties of low-e and solar control windows—simulations versus measurements, Solar Energy 69 (Suppl. 6) (2000) 15–26.
[12] D. Curcija, L.L. Ambs, W.P. Goss, A comparison of European and North American window $U$-value calculation procedures, ASHRAE Transactions 95 (1) (1989) 575–591.
[13] P. Blanusa, W.P. Goss, H. Roth, P. Weitzmann, C.F. Jensen, S. Svendsen, H. Elmahdy, Comparison between ASHRAE and ISO thermal transmittance calculation methods, Energy and Buildings 39 (2007) 374–384.
[14] A.H. Elmahdy, Assessment of spacer bar design and frame material on the thermal performance of windows, ASHRAE Transactions 112 (2) (2006) 30–43.
[15] A. Gustavsen, B.T. Griffith, D. Arastech, Natural convection effects in three-dimensional window frames with internal cavities, ASHRAE Transactions 107 (2) (2001) 527–537.
[16] P.F. de Abreu, R.A. Fraser, H.F. Sullivan, J.L. Wright, A study of insulated glazing unit surface temperature profiles using two-dimensional computer software, ASHRAE Transactions 102 (2) (1996) 497–507.
[17] D. Curcija, W.P. Goss, Two-dimensional finite-element model of heat transfer in complete fenestration systems, ASHRAE Transactions 100 (2) (1994) 1207–1221.
[18] S. Carpenter, A. McGowen, Effect of framing systems on the thermal performance of windows, ASHRAE Transactions 99 (1) (1993) 907–914.
[19] J.H. Klems, S. Reilly, Window nighttime $U$-values: a comparison between computer calculations and MOWITT measurements, ASHRAE Transactions 96 (1) (1990) 907–911.
[20] J.A. Baker, H.F. Sullivan, J.L. Wright, Window (glazing and frame) heat transfer modeling, ASHRAE Transactions 96 (1) (1990) 901–906.
[21] S.C. Carpenter, A.G. McGowan, Frame and spacer effects on window $U$-value, ASHRAE Transactions 95 (1) (1989) 604–608.

[22] F.M. Dubrois, S.J. Harrison, Comparison of experimental test results and analytical calculations of window performance, ASHRAE Transactions 95 (2) (1989) 747–754.
[23] R. Judkoff, J. Neymark, Model validation and testing: The methodological foundation of ASHRAE Standard 140, ASHRAE Transactions 112 (2) (2006) 367–376.
[24] R.D. Judkoff, Validation of building energy analysis simulation programs at the Solar Energy Research Institute, Energy and Buildings 10 (1998) 221–239.
[25] S.Ø. Jensen, Validation of building energy simulation programs: a methodology, Energy and Buildings 22 (1995) 133–144.
[26] K.J. Lomas, H. Eppel, C.J. Martin, D.P. Bloomfield, Empirical validation of building energy simulation programs, Energy and Buildings 26 (1997) 253–275.
[27] S. Moinard, G. Guyon, Empirical Validation of EDF ETNA and GENEC Test-Cell Models, A Report of Task 22, Project A.3 Empirical Validation, International Energy Agency, 1999.
[28] P.G. Loutzenhiser, G.M. Maxwell, A comparison of DOE-2.1E daylighting and HVAC system interactions to actual building performance, ASHRAE Transactions 112 (2) (2006) 409–417.
[29] G.M. Maxwell, P.G. Loutzenhiser, C.J. Klaassen, Daylighting—HVAC interaction tests for the empirical validation of building energy analysis tools, A Report of Task 22 Subtask D. Building Energy Analysis Tools Project D Empirical Validation. http://www.iea-shc.org/task22/reports/IEA%Daylighting%Report Final.pdf, 2003 (retrieved January 24, 2007).
[30] P. Strachan, Model validation using the PASSYS test cells, Building and Environment 28 (1993) 153–165.
[31] P. Wouters, L. Vandaele, P. Voit, N. Fisch, The use of outdoor test cells for thermal and solar building research within the PASSYS project, Building and Environment 28 (1993) 107–113.
[32] H. Manz, P. Loutzenhiser, T. Frank, P.A. Strachan, R. Bundi, G.M. Maxwell, Series of experiments for empirical validation of solar gain modeling in building energy simulation codes—experimental setup, test cell characterization, specifications and uncertainty analysis, Building and Environment 41 (2004) 1784–1797.
[33] P.G. Loutzenhiser, H. Manz, C. Felsmann, P.A. Strachan, T. Frank, G.M. Maxwell, Empirical validation of models to compute solar irradiance on inclined surfaces for building energy simulation, Solar Energy 18 (2007) 254–267.
[34] P.G. Loutzenhiser, H. Manz, P.A. Strachan, C. Felsmann, T. Frank, G.M. Maxwell, P. Oelhafen, An empirical validation of solar gain models found in building energy simulation programs, HVAC&R Research 12 (2006) 1097–1116.
[35] P.G. Loutzenhiser, H. Manz, C. Felsmann, P.A. Strachan, G.M. Maxwell, An empirical validation of modeling solar gain through a glazing unit with external and internal shading screens, Applied Thermal Engineering 27 (2007) 528–538.
[36] P.G. Loutzenhiser, H. Manz, S. Carl, H. Simmler, G.M. Maxwell, Empirical validations of solar gain models for a glazing unit with exterior and interior blind assemblies, Energy and Buildings 40 (2008) 330–340.
[37] EnergyPlus 1.2.3.023. A building energy simulation program, www.energyplus.gov, 2005.
[38] DOE-2.1E (Version-119). Building Energy Simulation Code, Lawrence Berkley Laboratories (LBL), Berkley, CA, April 9, 2002.
[39] IDA-ICE 3.0 Build 14. EQUA SA. Stockholm, Sweden, www.equa.se, 2005.
[40] European Standard EN 410. Glass in building—Determination of luminous and solar characteristics of glazing. European Committee for Standardization, Brussels, Belgium, 1998.
[41] BISCO Version 7.0w. A computer program to calculate 2D steady-state heat transfer, Physibel, Heirweg 21, B-9990 Maldegem, Belgium, 2004.
[42] prEN ISO 10077-2 Thermal performance of windows, doors and shutters—Calculation of thermal transmittance. Part 2: Numerical method for frames (Final Draft), European Committee for Standardization, Brussels, 2003.
[43] R. Perez, P. Ineichen, R. Seals, J. Michalsky, R. Stewart, Modeling daylight availability and irradiance components from direct and global irradiance, Solar Energy 44 (1990) 271–289.
[44] EnergyPlus, Input Output Reference, Board of Trustees of University of Illinois and the University of California through Orlando Lawrence Berkley Laboratories (October 11, 2005).
[45] Window 5.2 Version 5.2.17a., Code to calculate window properties, LBL, http://windows.lbl.gov/software/window/window.html, 2005.
[46] M. Rubin, K. Von Rottkay, R. Powles, Window optics, Solar Energy 65 (1998) 149–161.
[47] ASHRAE, ASHRAE Fundamentals 2001 SI Edition, American Society of Heating, Refrigeration and Air-Conditioning Engineers, Inc, Atlanta, GA, USA, 2001.
[48] ISO/FDIS 15099: 2003(E), Thermal performances of windows, doors and shading devices—Detailed calculations, 2003.
[49] I. Beausoleil-Morrison, P. Strachan, On the significance of modeling internal surface convection in dynamic whole-building simulation programs, ASHRAE Transactions 105 (2) (1999) 929–940.